A mixed implicit–explicit finite difference scheme for heat transport in magnetised plasmas

S. Günter *, K. Lackner

Max-Planck-Institut für Plasmaphysik, EURATOM Association, Boltzmannstrasse 2, 85748 Garching, Germany

ABSTRACT

An explicit/implicit domain decomposition method is applied to the time-dependent heat-conduction problem in a 2-d, strongly anisotropic medium (a magnetised plasma), using a formulation of the spatial derivatives which avoids the pollution of perpendicular by parallel heat fluxes. The time-stepping at the sub-domain boundaries is done using a DuFort–Frankel scheme, which leads to a time step limit given not by instabilities, but by the damping rate of numerical oscillations driven by inconsistencies in the formulation of initial conditions or the temporal variations in the true physical solution. These limitations can be minimized, however, by aligning the subdomain boundaries as much as possible with magnetic flux surfaces. The time step limit depends on the ratio of the implicit grid spacing to the distance between subdomain boundaries (DuFort–Frankel lines in 2-d, surfaces in 3-d).

© 2008 Elsevier Inc. All rights reserved.

1. Introduction

The modelling of conductive heat transport in magnetised plasmas is a central theme in thermonuclear fusion research, rendered highly demanding by the extreme anisotropy of the heat conductivity. In previous papers [1,2] we have outlined several variants of a numerical scheme which minimizes the pollution of the weak heat fluxes perpendicular to magnetic field lines, by the potentially much more efficient transport along them (typical ratio of heat conductivities in the core of a present tokamak experiment $\chi_{//}/\chi_{\perp} > 10^{10}$). In fact this scheme has been successfully applied to realistic situations, like the 3-d problem of heat transport across magnetic islands and in ergodic layers [3]. In Refs. [1,2] we considered the solution to the stationary problem, arguing that the same treatment of the spatial derivatives could be used in implicit formulations of the time-dependent equation. In fact this has been successfully done in Refs. [4,5]. As these solutions sometimes develop boundary layers – e.g. along the border of magnetic islands – frequently a very high spatial resolution is required, making, at least in 3-d, the resulting matrices of very demanding or even prohibitive size. At the same time such a fully implicit scheme is difficult to implement on highly parallel systems.

Recently Yuan and Zuo [6] have analysed a hybrid explicit/implicit algorithm similar to one previously proposed by Black [7], which naturally decomposes the computational domain into sub-domains. The time evolution at the sub-domain interfaces is calculated using a DuFort–Frankel (DF) scheme, and the results used as Dirichlet boundary condition data for the implicit formulation within the sub-domains. The authors showed this scheme to be unconditionally stable, and presented results of a sample application to a 1-d problem. Evidently, this algorithm, applied in 2 or 3 dimensions, substitutes one large by a set of much smaller matrices, and is intrinsically predisposed for domain decomposition. In the present paper we

* Corresponding author. Tel.: +49 89 3299 1718; fax: +49 89 3299 2580.
E-mail address: guenter@ipp.mpg.de (S. Günter).

combine these ideas with the spatial discretisation of Ref. [1], and apply it to the time dependent, anisotropic heat transport in 2-d, magnetised plasmas. While the scheme is, as shown by Yuan and Zuo, unconditionally stable, the DF algorithm applied at the sub-domain boundaries is prone to the excitation of weakly damped oscillations, driven either by rapid variations in the applied sources, or an inconsistent initialisation of the calculations. These oscillations are, however, much stronger damped in this case than in a pure DF scheme, and can be controlled, provided the time step is chosen according to criteria given in the present paper.

2. Mixed implicit–explicit formulation in 2-d geometry

We describe the generalization of the numerical scheme proposed in Ref. [6] to the anisotropic problem of heat conduction in magnetised plasmas using 2-d cylindrical coordinates (r, θ) over a radial interval $0 \leqslant r \leqslant 1$. We had used this geometry in Refs.[1,2] to develop and test a spatial discretisation scheme minimizing pollution of the small heat transport perpendicular to field lines (in this geometry equivalent to flux surfaces) by the much larger one parallel to them. As argued in Ref. [1] it is expedient to have coordinate lines of one coordinate (here: r) coincide approximately with flux surfaces, which can be achieved in the general case by aligning the system with the unperturbed field. This had been subsequently implemented in Ref. [3] for a 3-d magnetic field configuration, albeit still based on zero-order circular, cylindrical flux surfaces. In Ref. [4] the geometry was further generalized to the realistic case of a toroidal plasma with the non-circular unperturbed flux surfaces, corresponding to an existing tokamak. In the latter case, non-orthogonal coordinates were used, with the unperturbed flux surfaces taken as effectively radial coordinate surfaces. Cylindrical coordinates, with 2-d magnetic field configurations and finite B_r have thus been shown to be a good model system for the numerical treatment of more realistic problems of anisotropic heat transport.

We focus on the treatment of the electron heat conduction term, and write the temperature evolution equation in the form

$$\frac{3}{2} n_e \frac{\partial}{\partial t} T = -\nabla \cdot \vec{q} + Q, \tag{1}$$

with n_e being the electron density and Q the heat source, neglecting terms arising from convection and compression heating. For strongly magnetised plasmas, the main difficulties arise from the term involving the parallel transport in the heat flux

$$\vec{q} = -n_e[\chi_{//}\vec{b}\vec{b} + \chi_{\perp}(\overleftrightarrow{I} - \vec{b}\vec{b})] \cdot \nabla T. \tag{2}$$

In our previous papers we considered a fully implicit solution of the heat conduction equation. To reduce the size of the involved matrices, we decompose the computational domain here into N_r sub-domains by introducing domain boundaries at various radii r_i, $i = 1, 2, \ldots, N_r$. Inside these sub-domains, we apply an implicit scheme

$$\frac{3}{2} n_e \frac{T^{n+1} - T^n}{\Delta t}\bigg|_{i,j} = -\frac{\{\vec{e}_r, 0\}}{2r_i\Delta r}(r_{i+1/2}(\vec{q}^{n+1}_{i+1/2,j+1/2} + \vec{q}^{n+1}_{i+1/2,j-1/2}) - r_{i-1/2}(\vec{q}^{n+1}_{i-1/2,j+1/2} + \vec{q}^{n+1}_{i-1/2,j-1/2})) - \frac{\{0, \vec{e}_\theta\}}{2r_i\Delta\theta}(\vec{q}^{n+1}_{i+1/2,j+1/2}$$
$$+ \vec{q}^{n+1}_{i-1/2,j+1/2} - \vec{q}^{n+1}_{i+1/2,j-1/2} - \vec{q}^{n+1}_{i-1/2,j-1/2}) + Q^n_{ij}, \tag{3}$$

defining the parallel heat fluxes at intermediate grid points following the prescription of Ref. [1].

$$\vec{q}^{n+1}_{\|,i+1/2,j+1/2} = -n_e\chi_\|\vec{b} \cdot (\vec{b} \cdot \nabla_r T + \vec{b} \cdot \nabla_\theta T)|^{n+1}_{i+1/2,j+1/2}$$
$$= -n_e\chi_\|\{b^r, b^\theta\}|_{i+1/2,j+1/2} \begin{pmatrix} b^r_{i+1/2,j+1/2} \frac{(T^{n+1}_{i+1,j+1}+T^{n+1}_{i+1,j}-T^{n+1}_{ij+1}-T^{n+1}_{ij})}{2(\Delta r)_I} + \\ b^\theta_{i+1/2,j+1/2} \frac{(T^{n+1}_{i+1,j+1}+T^{n+1}_{ij+1}-T^{n+1}_{i+1,j}-T^{n+1}_{ij})}{2\Delta\theta r_{i+1/2}} \end{pmatrix} \tag{4}$$

In this and following equations, we add an index I to the radial step size, to indicate the interval between neighbouring implicitly treated points. At the sub-domain boundaries, the heat conduction equation is solved in an explicit way by

$$\frac{3}{2} n_e \frac{T^{n+1} - T^{n-1}}{2\Delta t}\bigg|_{i,j} = -\frac{\{\vec{e}_r, 0\}}{2r_i(\Delta r)_I}(r_{i+1/2}(\vec{q}'^m_{i+1/2,j+1/2} + \vec{q}'^m_{i+1/2,j-1/2}) - r_{i-1/2}(\vec{q}'^m_{i-1/2,j+1/2} + \vec{q}'^m_{i-1/2,j-1/2}))$$
$$- \frac{\{0, \vec{e}_\theta\}}{2r_i\Delta\theta}(\vec{q}'^m_{i+1/2,j+1/2} + \vec{q}'^m_{i-1/2,j+1/2} - \vec{q}'^m_{i+1/2,j-1/2} - \vec{q}'^m_{i-1/2,j-1/2}) + Q^n_{ij}. \tag{5}$$

The relevant heat fluxes q' involved at the sub-domain boundaries are calculated using a generalisation of the DuFort–Frankel scheme:

$$\vec{q}'^m_{\|,i+1/2,j+1/2} = -n_e\chi_\|\{b^r, b^\theta\}|_{i+1/2,j+1/2} \begin{pmatrix} b^r_{i+1/2,j+1/2} \frac{1}{2(\Delta r)_I}(T^n_{i+1,j+1} + T^n_{i+1,j} - \frac{1}{2}(T^{n+1}_{ij+1} + T^{n+1}_{ij} + T^{n-1}_{ij+1} + T^{n-1}_{ij})) + \\ b^\theta_{i+1/2,j+1/2} \frac{1}{2r_{i+1/2}\Delta\theta}(T^n_{i+1,j+1} + T^n_{ij} - \frac{1}{2}(T^{n+1}_{ij+1} + T^{n+1}_{ij} + T^{n-1}_{ij+1} + T^{n-1}_{ij})) \end{pmatrix}. \tag{6}$$
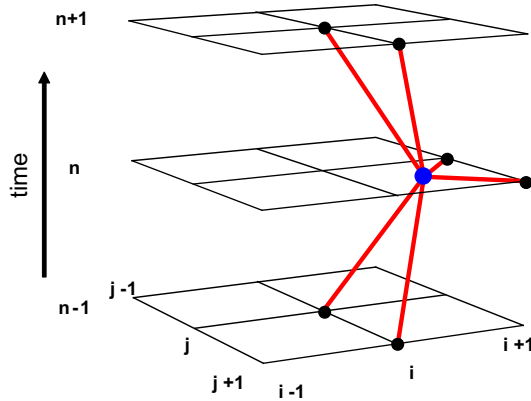
Fig. 1. Grid points involved in the computation of the heat fluxes at point $(i + 1/2, j + 1/2)$ required for the DuFort–Frankel scheme used along the sub-domain boundary at $r = r_i$ (along the "DuFort–Frankel line").

The grid points involved in the computation are outlined in Fig. 1. N_{DF} implicit intervals (Δr_I) are between adjacent DF-points, so that at constant spatial resolution (Δr_I) the number of subdomains will scale like N_{DF}^{-1}. As in our previous papers, all heat fluxes are defined in the intermediate grid point, whereas temperatures are defined in integer grid points. This treatment ensures that no strong pollution of the perpendicular heat flux is caused by the parallel one even for large values of $\chi_{\|}/\chi_{\perp}$ and non-aligned magnetic coordinates as already proven for the full implicit scheme developed in Refs. [1,2]. The solution at the sub-domain boundaries gives the Dirichlet boundary condition applied for the implicit scheme in the sub-domain interior.

Eqs. (1)–(5) are written in the form of Refs. [1,2] to highlight how variable coefficients enter the difference formulation. In the following we chose a normalisation dropping the 3/2 in front of the temperature time derivative, and set $n_e = \text{const.} = 1$. For 2-d calculations in the (r, θ)-plane, we define the magnetic field through a flux function $\vec{B} = \vec{e}_z \times \nabla \psi$, which for the 2-d test applications in this paper is given by

$$\psi(r, \theta) = (r - r_s)^2 + 0.005 r^2 (1 - r^4) \cos \theta, \tag{7}$$

resulting in a magnetic island at the rational surface r_s (=0.7). We use $T(r = 1, \theta, t) = 0$, $T(r, \theta, t = 0) = 0$ as boundary and initial condition and – for the reference case – a source given by $Q = 4(1 - r^2)^8 \tanh(t/\tau_s)$. The ramping-up of the source, with a time-constant τ_s is imposed so that the additional unphysical condition on $\partial T/\partial t$ (taken as = 0) needed to initiate the algorithm in the DF-points, is consistent with the actual solution of the problem.

For the reference case, shown in Figs. 2 and 3 we chose $\chi_{//}/\chi_\perp = 10^7$, keeping in mind that in a 2-d simulation this parameter is an effective value, related to the true one by the relation $(\chi_{//}/\chi_\perp)_{2d} = (\chi_{//}/\chi_\perp)_{3d} \cdot (B_r^2 + B_\theta^2)/(B_r^2 + B_\theta^2 + B_z^2)$, and hence to be taken more than two orders of magnitude smaller to simulate tokamak conditions [2]. The implicit step sizes are taken as $(\Delta r)_I = 0.0033$ and $(\Delta \theta)_I = 0.025$, with $N_{DF} = 15$, and a time step $\Delta t = 0.003$. The spatial resolution is needed to reproduce
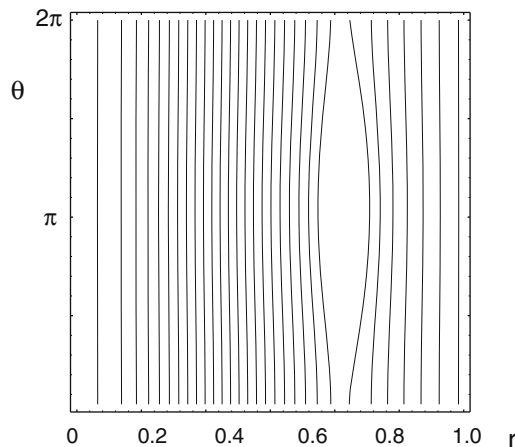

Fig. 2. Temperature contours for the asymptotic solution ($t = 3.9$) of our reference case, in a projection on a plane r, θ system.
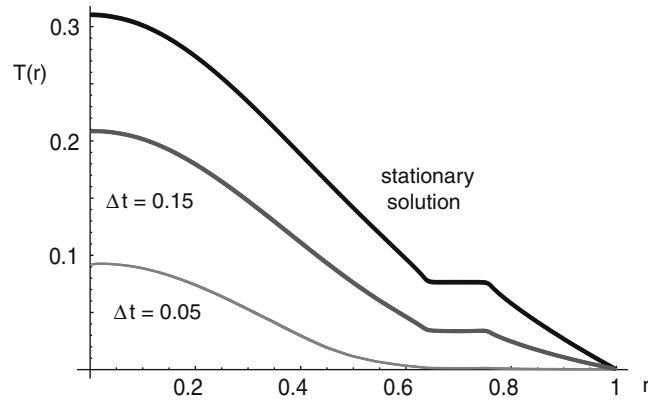
Fig. 3. Radial profiles of temperature through the *O*-point of the island for the reference case, during the build-up ($t = 0.05, 0.15$) and at $t = 3.9$.

the sharp transition zone at the island boundary. Fig. 2 shows the isocontours of temperature in the asymptotic state, whereas Fig. 3 shows radial profiles through the O-point of the island, during the build-up and at a late (asymptotic) state.

3. Constraints on the utilizable time-step

The above and several other test cases showed that the mixed scheme of Ref. [6] can indeed be implemented in a satisfactory way also in more than one dimension, to solve the strongly anisotropic heat conduction problem in magnetic fields. The generally known drawbacks of the DF scheme, and the adjustable parameters of the above mixed scheme ($(\Delta x)_I, \Delta t$, but in particular N_{DF}, however, made extensive numerical tests mandatory. To guide our understanding and to arrive at a scaling of the useable time steps Δt supported by an at least heuristic model, we explored also more extensively the 1-d situation, already discussed in the paper of Yuan and Zuo [6].

The DuFort–Frankel scheme for the heat conduction equation is known to be unconditionally stable for proper boundary conditions. Yuan and Zuo [6] have shown that this general property holds also for the combined DF-explicit, implicit scheme. In practice, however, the DF method is known to suffer from the danger of the excitation of weakly damped oscillations, e.g. by too rapidly varying sources or by inconsistent initial conditions. Related to this is the fact that the DF scheme modifies the basic type of the partial differential equation, introducing a hyperbolic term vanishing only for $(\Delta t/\Delta x) \to 0$. We show in the following that the mixed scheme of Ref. [6] has indeed much superior properties. To illustrate this, we consider at first the 1-d analogue to our 2-d problem, solving the standard heat conduction equation in the form

$$\frac{\partial}{\partial t}T = \chi \frac{1}{r}\frac{\partial}{\partial r}r\frac{\partial}{\partial r}T + Q/n_e, \tag{8}$$

with $\chi = 1$, the same source distribution and initial and boundary conditions as above, albeit necessarily with only a perpendicular heat conductivity, and no equivalent of magnetic islands. Similar to the above case (for the reasons discussed in the
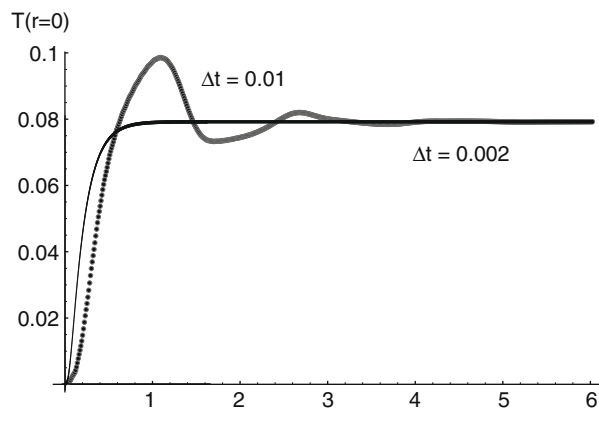

Fig. 4. Time development of $T(r = 0, t)$ in a 1-d case, with $(\Delta r)_I = 0.0025$, $N_{DF} = 40$, and time steps $\Delta t = 0.002$ (solid line) and $=0.01$ (dotted), respectively.
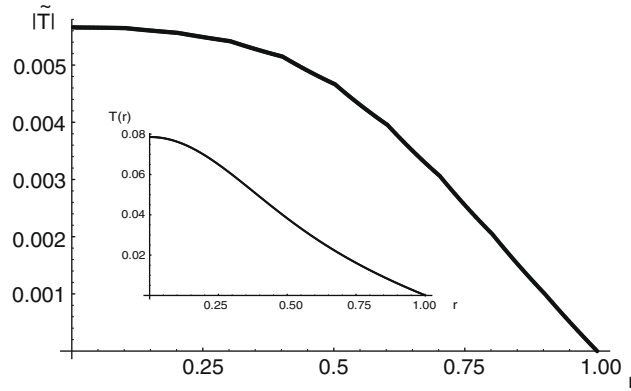
Fig. 5. Radial profile of the perturbation $\widetilde{T}(r, t = 1.8)$ for a time step $\Delta t = 0.01$. The insert shows the true solution in the asymptotic state.

subsequent section) we ramp-up the source with a time-function $\sim \tanh(t/\tau_s)$. For a too large time step (Fig. 4) the true solution $T(r, t)$ is overlaid by a damped temporal oscillation $\widetilde{T}(r, t)$, with a radial scale length ~ 1 (Fig. 5). Closer inspection reveals, however, that the function $\widetilde{T}(r, t)$ actually constitutes a polygon in r, with pivots in the DuFort–Frankel points. This behaviour can be understood from an inspection of the PDE's obtained as differential approximations to the difference schemes [8], which take the form

$$\frac{\partial}{\partial t}T = \chi\frac{\partial^2}{\partial x^2}T - \chi\left(\frac{\Delta t}{(\Delta x)_I}\right)^2\frac{\partial^2 T}{\partial t^2} \tag{9}$$

for the case of the DF-scheme, and

$$\frac{\partial}{\partial t}T = \chi\frac{\partial^2}{\partial x^2}T + \frac{\Delta t}{2}\chi\frac{\partial}{\partial t}\frac{\partial^2 T}{\partial x^2}, \tag{10}$$

for the implicitly treated regions. (To focus on the essentials, we carry-out this discussion, as well as the analysis given in the Appendix in plane geometry, and ignore the source terms).

In the mixed formulation described in Section 2, Eq. (9) is solved in the region $x_{DF,i} - (\Delta x)_I/2 \leqslant x \leqslant x_{DF,i} + (\Delta x)_I/2$ around each DF point $x_{DF,i}$, whereas Eq. (10) is solved in the remainder of the computational domain. Defining a function $g(x)$ as 1 inside and 0 outside the region of validity of (9), the perturbation $\widetilde{T}(x, t)$ has to satisfy an equation of the form

$$\frac{\partial}{\partial t}\widetilde{T} = \chi\frac{\partial^2}{\partial x^2}\widetilde{T} - g(x)\chi\left(\frac{\Delta t}{(\Delta x)_I}\right)^2\frac{\partial^2}{\partial t^2}\widetilde{T} + (1 - g(x))\frac{\Delta t}{2}\chi\frac{\partial}{\partial t}\frac{\partial^2\widetilde{T}}{\partial x^2} - g(x)\chi\left(\frac{\Delta t}{(\Delta x)_I}\right)^2\frac{\partial^2}{\partial t^2}T + (1 - g(x))\frac{\Delta t}{2}\chi\frac{\partial}{\partial t}\frac{\partial^2 T}{\partial x^2}, \tag{11}$$

where the last two terms describe the drive of the oscillations by the time-variation of the true solution $T(x, t)$.

In the Appendix we describe a semi-heuristic method by which we use the observed spatial structure of the perturbations in our numerical experiment to derive a time-dependent solution for the homogeneous part of Eq. (11), which predicts a behaviour $\widetilde{T}(x, t) \sim G(x) \cdot e^{\gamma t + i\omega t}$, with

$$\begin{aligned}\gamma &= -c_1\frac{(\Delta x)_I^2 N_{DF}}{2\chi(\Delta t)^2} \\ \omega &= c_2\frac{(\Delta x)_I\sqrt{2N_{DF}}}{\ell(\Delta t)},\end{aligned} \tag{12}$$

with ℓ a characteristic spatial scale of the perturbation (in the case of the mode observed in Fig. 5, the total extent of the computational region) and c_1, c_2 constants of $O(1)$. For comparison, a spectral mode ansatz for the perturbation in terms of a spatial wave-number k for a pure DF-scheme would yield:

$$\begin{aligned}\gamma_{DF} &= -\frac{(\Delta x)_{DF}^2}{2\chi(\Delta t)^2} \\ \omega &= \frac{(\Delta x)_{DF}k}{(\Delta t)}.\end{aligned} \tag{13}$$

Comparing the two expressions (in particular those for the damping rate $-\gamma$), one should note that the requirement to resolve a certain spatial scale will impose a fixed $(\Delta x)_I$, whereas the number of subdomains will be a parameter to optimize, taking into account a given computer architecture. For a fixed time step and a given spatial resolution the rate of damping will therefore be larger by a factor N_{DF} for the hybrid scheme than for the pure DF treatment.

The scaling of damping rate and oscillation frequency implied by Eq. (12) are very well reproduced by our numerical tests carried out in 1-d, but holds approximately also in 2-d simulations. Figs. 6 and 7 show, for the 1-d case, the excellent agree-
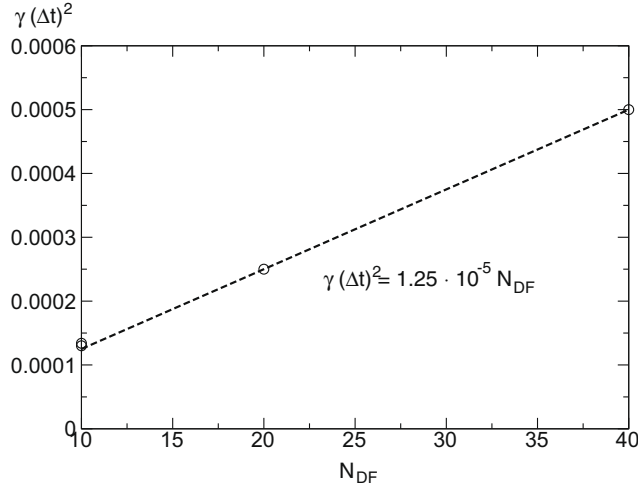
Fig. 6. Results of numerical tests (circles) and the prediction of Eq. (12) (dashed line) for the damping rate of the perturbation $\widetilde{T}(r = 0, t)$. Shown is $\gamma \cdot (\Delta t)^2$ as function of N_{DF} (no correction factor applied).

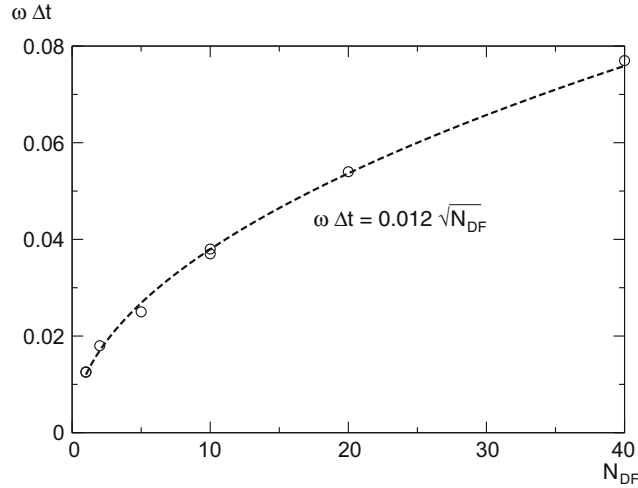**Fig. 7.** Results of numerical tests (circles) and the prediction of Eq. (12) (dashed line) for the oscillation frequency of the perturbation $\widetilde{T}(r = 0, t)$. Shown is $\omega \cdot (\Delta t)$ as function of N_{DF}. The dashed curve corresponds to Eq. (12) for a value of $\ell = 0.59$.

ment of the scaling of the characteristic frequency and damping rate of these perturbations with the predictions of Eq. (12). In the case of the damping rate, this agreement extends also to the numerical value; the measured frequencies are uniformly about 40% higher than those predicted by Eq. (12) for $\ell \sim 1$. This is not surprising, as the spatial structure of the perturbation is not exactly a parabola (as assumed in the Appendix) and the analytic expression obtained there also refers to a plane geometry. The predicted damping rate, on the other hand, does not even depend on the spatial scale of the perturbation and should therefore also be more robust with regard to its detailed structure.

In 2-d, the role of anisotropy $\chi_{//}/\chi_{\perp}$, and the dependence of the solution on the structure of the magnetic field $\vec{B}(r, \theta)$ complicate the matter. Also here, for too large time-steps, oscillations appear (Fig. 8). They have a more complex time-behaviour, as evidently the larger number of degrees of freedom allows for more than one oscillation mode to be excited. The spatial structure of the perturbation (Fig. 9: isocontours of $\widetilde{T}(r, \theta, t = 3.9)$, obtained as difference between the solutions with $\Delta t = 3 \cdot 10^{-3}$ and $5 \cdot 10^{-4}$, respectively at this instance) closely resembles that of the true solution (Fig. 2). This similarity is illustrated more quantitatively by radial cuts of $\widetilde{T}(r, \theta, t = 3.9)$, through the O- and X-points of the island (Fig. 10), which manifest also the polygonal structure. We carried out again a variety of numerical simulations testing the scaling of damping rate and oscillation frequency of these perturbations, with results shown in Figs. 11–14. For applying the Eq. (12) we had to define a reference heat conductivity, which we took as the spatial maximum of $\chi_{ref} = \max(1 + (b_r)^2(\chi_{//}/\chi_{\perp}))$. The latter quantity appears as coefficient of the second time derivative in the 2-d generalisation of Eq. (11), making it clear also
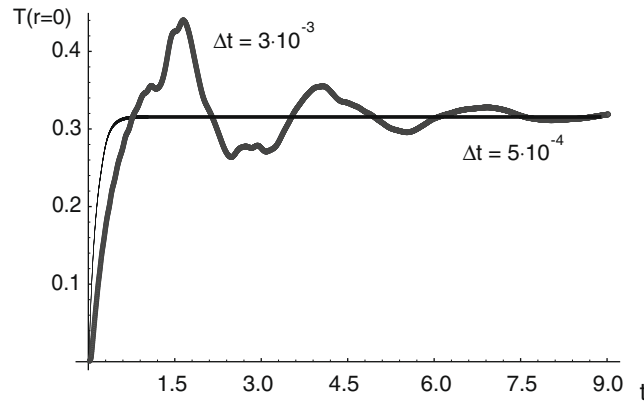
Fig. 8. Time development of $T(r = 0, t)$ in the 2-d reference case, for time steps $\Delta t = 3 \cdot 10^{-3}$ and $5 \cdot 10^{-4}$, respectively.
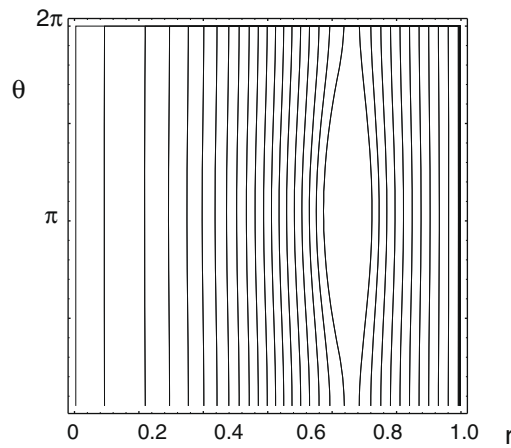

Fig. 9. Isocontours of $\widetilde{T}(r, \theta, t = 3.9)$, obtained as difference between the solutions with $\Delta t = 3 \cdot 10^{-3}$ and $5 \cdot 10^{-4}$, respectively.
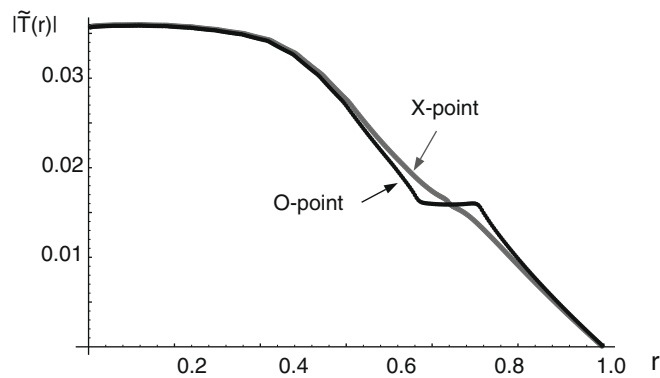

Fig. 10. Radial cuts of $\widetilde{T}(r, \theta, t = 3.9)$, for $\Delta t = 3 \cdot 10^{-3}$ through the O- and X-points of the island.

why the DuFort–Frankel treatment should be with respect to a coordinate perpendicular to the unperturbed flux surfaces. (A further profit should accrue if DuFort–Frankel surfaces can be placed on still intact flux surfaces, like KAM-surfaces). As can be seen the damping rates still scale in reasonable agreement with Eq. (12), with a somewhat weaker dependence on $\chi_{//}/\chi_{\perp}$, which is, however, to be expected as over large parts of the computational region the actual value of χ_{ref} stays closer to 1. A
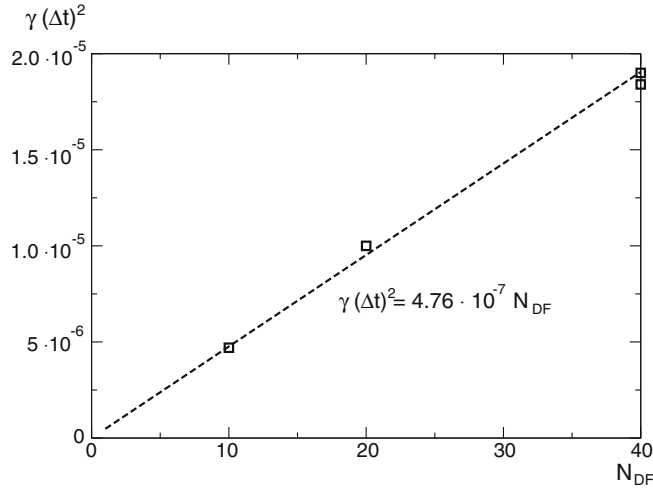
Fig. 11. Damping rate γ of slowest decaying fluctuations from 2-d calculations (squares) with different $\Delta t, N_{DF}$, for $\chi_{//}/\chi_{\perp} = 10^7$, corresponding, for the magnetic configuration used, to a $\chi_{ref} = 41$. The dashed line corresponds to $\gamma \cdot (\Delta t)^2 = 4.8 \cdot 10^{-7} N_{DF}$, whereas a straightforward evaluation of Eq. (12) predicts $3 \cdot 10^{-6} N_{DF}$.
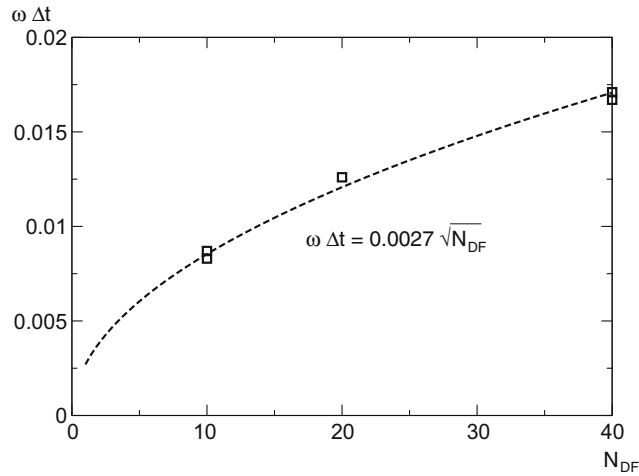

Fig. 12. Oscillation frequency ω (squares) of slowest decaying fluctuations for the cases of the dot-dashed curve corresponds to $\omega \cdot (\Delta t) = 0.0027\sqrt{N_{DF}}$.

stronger deviation is observed for the oscillation frequency, which according to Eq. (12) should be independent of χ_{ref}, but is found to scale $\sim \chi_{ref}^{-0.4}$. This is presumably due to the fact that the 2-d structure of the solution (and also the perturbation) gets increasingly more pronounced with increasing $\chi_{//}/\chi_{\perp}$.

The above tests refer to cases, in which the time variation of the true, physical solution of Eq. (1) drives the numerical oscillations, with a spatial distribution given either by the global scale, or – in case of the sudden switch-on of a spatially more restricted source (in practice, e.g. the application of ECRH-heating) – a smaller scale ℓ. The best confirmation of the range of applicability of the expressions Eq. (12) was, however, obtained by 1 and 2-d runs with improper initialisation, taking, from the very beginning of the calculations a finite source strength $Q(r, t)$, but initiating the DF points with $T(r_{DFj}, \theta, -\Delta t) = T(r_{DFj}, \theta, 0) = 0$. This led to strong oscillations with a characteristic dimension $\ell \sim (\Delta r)_{DF}$, with the same damping rate as the global oscillations, but a frequency scaling now like $\omega \cdot (\Delta t) \sim \sqrt{(\Delta r)_l/(\Delta r)_{DF}}$.

One remarkable property of Eq. (12) is the fact that the damping rate for the induced numerical oscillations is independent of their spatial scale. This implies that the problem will lead to more severe time-step limitations if smaller scale physical variations are to be resolved. As practical criterion we can formulate that the damping of numerical oscillations should be on a shorter time-scale than the physical one. Taking – for a physical perturbation on a scale ℓ the associated physically relevant time scale as $\tau_\ell \approx \ell^2/\chi$, this requests:
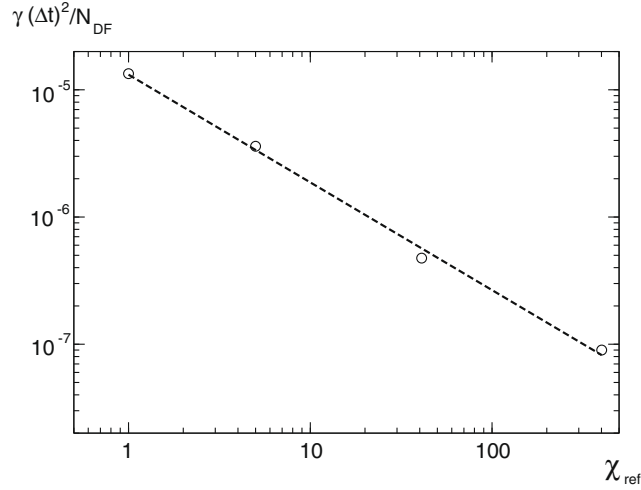
$\gamma\,(\Delta t)^2/N_{DF}$

Fig. 13. Scaling of the damping rate of the slowest decaying mode with χ_{ref} for various $\Delta t, N_{DF}$ in logarithmic representation. The dashed line corresponds to $\gamma\cdot(\Delta t)^2/N_{DF}\sim\chi_{ref}^{-0.85}$.
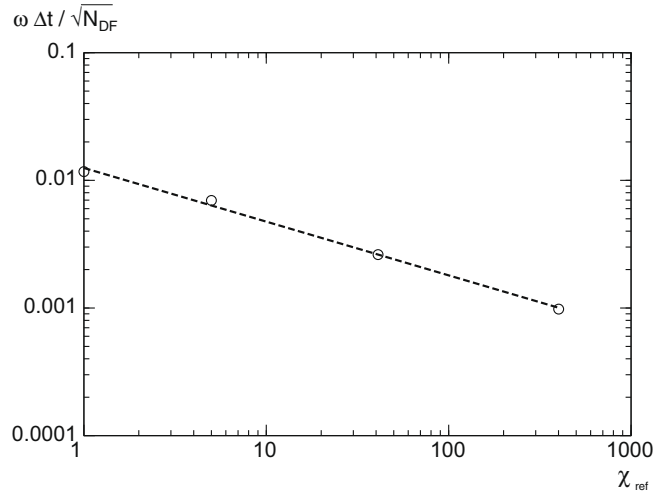
$\omega\,\Delta t/\sqrt{N_{DF}}$

Fig. 14. Scaling of the oscillation frequency of the slowest decaying mode with χ_{ref} for various $\Delta t, N_{DF}$ in logarithmic representation. The dashed line corresponds to $\omega\cdot(\Delta t)/\sqrt{N_{DF}}\sim\chi_{ref}^{-0.42}$.

$-\gamma\tau_\ell\approx c_1\frac{(\Delta x)_I(\Delta x)_{DF}\ell^2}{2\chi^2(\Delta t)^2}>1$, which can be reformulated as a time-step criterion:

$$\Delta t<\frac{(\Delta x)_I\ell}{\chi}\sqrt{\frac{c_1}{2}N_{DF}}. \tag{14}$$

Another form of a time-step criterion can be derived by demanding that the oscillations excited with a spatial scale ℓ should be critically damped: using the expressions of Eq. (12) this requirement $-\gamma/\omega>1$ takes – up to a factor $\sqrt{c_1}/(2c_2)$- again the same form as Eq. (14).

To test this conclusion numerically in the 1-d case we imposed a source that produces asymptotically a spatially localized temperature distribution $T(r,t\to\infty)=e^{-(r-0.5)^2/\sigma^2}$. Taking for this case and $(\Delta r)_I=0.0025, N_{DF}=40$ a time-step $\Delta t=10^{-3}$, which would be sufficient to produce a monotonic approach to the asymptotic solution for the model source distribution used in the earlier tests, yields a temporal behaviour of $T(0,t)$ with a strong oscillation overlaid to the physical excursion (Fig. 15). An oscillation persists also for a time-step reduced by a factor of 2; a time step of 1/4th of the original one suffices, however, to give essentially the physically correct solution, approximately in agreement with the ratio of the space-scales of the dominating perturbations for the two cases (Figs. 5 and 16). For ramp-up rates exceeding a few (less than 10) Δt, these oscillations do not depend on the rate of rise of the source.

Expression Eq. (12) explains also the particular importance of a consistent start-up of the calculations. As the DF points require a specification also of the time derivative of $T(r,\theta,t=0)$, any specification not consistent with the actual solution
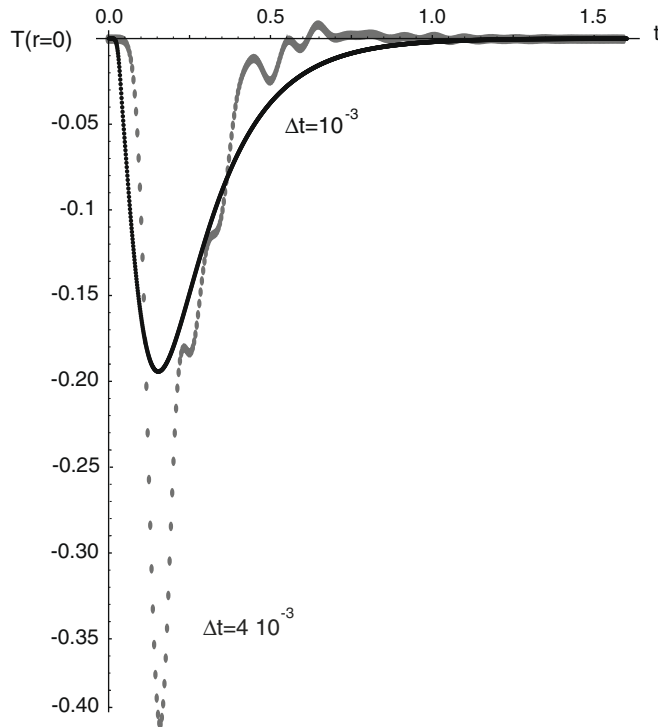
Fig. 15. 1-d solution for a narrow source: $T(0, t)$ for time steps of $\Delta t = 4 \cdot 10^{-3}$ (dashed line) and 10^{-3} (solid line).
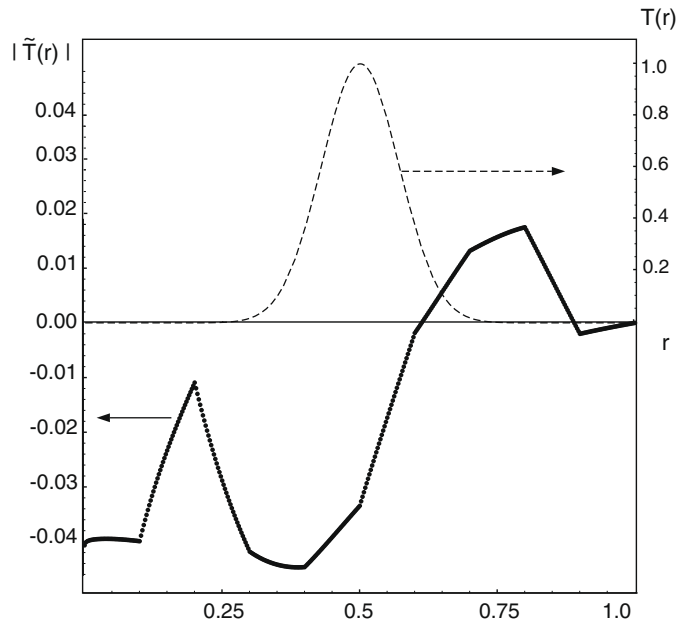

Fig. 16. Profile of the perturbation $\widetilde{T}(r, t = 0.26)$ for the case of Fig. 15 and $\Delta t = 4 \cdot 10^{-3}$. Insert: stationary solution.

excites a perturbation with a spatial scale $\ell \sim N_{\mathrm{DF}}(\Delta r)_I$, posing a rather stringent requirement for critical damping. Our meth-od – to start with $T(r, \theta, t = 0) = 0$, $\partial T(r, \theta, t = 0)/\partial t = 0$, and to ramp-up the source from initially uniformly zero to its in-tended value within a few Δt was, however, very successful in eliminating this problem. It is in fact, of more general applicability than might appear apparent. Due to the linearity of the problem, it can be applied to start-up with any initial distribution $T(r, \theta, t = 0) = T_o(r, \theta)$ for any source distribution $Q(r, \theta, t)$, by obtaining first, through differentiation, a fictitious

source $Q_s(r, \theta)$, satisfying the stationary heat conduction equation for $T_o(r, \theta)$ and applying the algorithm described in this paper, using a source $Q_s + (Q - Q_s) \cdot \tanh(t/\tau_s)$. Evidently, in that case, $\partial T(r, \theta, t = 0)/\partial t = 0$ gives an initialisation in the DF-points consistent with the actual solution of the PDE.

4. Conclusions

We have shown that the mixed explicit/implicit scheme proposed by Yuan and Zuo can be successfully combined with the spatial discretisation of Günter et al. for the solution of 2-d, strongly anisotropic heat conduction problems, provided certain constraints on the time step are respected. We expect this to hold also in 3-d, and efforts for the practical implementation into the code described in Refs. [3,5] are under way. The method breaks the original coefficient matrix for the solution at the new time-step, with $\approx 27 \cdot N_x \cdot N_y \cdot N_z$ non-vanishing entries, into N_x/N_{DF} matrices with each $\approx 27 \cdot N_{DF} \cdot N_y \cdot N_z$ elements, leaving the total number of elements approximately constant, but evidently facilitating their distribution and parallel solution on several nodes. The method appears ideally suited for problems of perturbed, magnetically confined plasmas, where a fully implicit treatment on the nested magnetic surfaces of the original equilibrium configuration can be combined with a mixed implicit–explicit treatment along the coordinate perpendicular to them. The method is unconditionally stable, but imposes a time-step constraint of the type

$(\Delta t)_{\max} \propto \frac{(\Delta x)_I \ell}{\chi_{\mathrm{eff}}} \sqrt{N_{DF}}$ to avoid spurious oscillations of the solution, where χ_{eff} is an effective heat conductivity perpendicular to the boundaries of the fully-implicitly treated subdomains. It is approximately given by $\chi_{\mathrm{eff}} = \chi_\perp (1 + (b_r)^2 (\chi_{//}/\chi_\perp))$, and illustrates also the benefit derived from an approximate alignment of the subdomain boundaries with the unperturbed flux surfaces.

Appendix

To obtain practical guidance for the choice of the time-step Δt and the number of DF points, lines or surfaces, respectively in 1, 2, or 3 dimensions, we need to relate these parameters to the observed temporal oscillations. The heuristic analysis described below refers to a 1-d situation, and derives the justification of its use in the more general 2-d case from the numerical tests and the comparison of their results.

We start from the homogenous part of Eq. (11)

$$\frac{\partial}{\partial t} \widetilde{T} - \chi \frac{\partial^2}{\partial x^2} \widetilde{T} + g(x) \chi \left(\frac{\Delta t}{\Delta x} \right)^2 \frac{\partial^2}{\partial t^2} \widetilde{T} - (1 - g(x)) \frac{\Delta t}{2} \chi \frac{\partial}{\partial t} \frac{\partial^2 \widetilde{T}}{\partial x^2} = 0, \tag{A1}$$

with the definition of $g(x)$ given in Section 3. We apply separation in time and investigate a particular spatial perturbation with a global scale-length ℓ, using the numerical observation of $\widetilde{T}(x, t)$ taking the spatial shape of a polygon with vanishing $\frac{\partial^2}{\partial x^2} \widetilde{T}$ over the region with $g = 0$. We therefore make an ansatz $\widetilde{T}(x, t) = \widetilde{T}_o(t) \cdot G(x)$, with $G(x)$ defined as polygon, with pivots in the DF-points, given by $G(x_{DF j}) = (1 - (x_{DF j}/a)^2)$. This corresponds approximately to the oscillating perturbation in Fig. 5. We use the function $G(x)$ now also as trial function in a Galerkin approach, multiplying Eq. (A1) with it and integrating over the interval $[0, a]$. Evaluating the first and second terms gives only $((\Delta x)_{DF}/a)^2$-corrections to the expressions for the continuous function $(1 - (x/a)^2)$. The fourth term vanishes for the chosen trial function. The essential features of the DF enter through the third term, whose contribution is attenuated, however, by the small interval around the DF points over which $g(x) \neq 0$. By this procedure, the PDE (A1) becomes a second order DE in time

$$\frac{2}{3} \chi \left(\frac{\Delta t}{(\Delta x)_I} \right)^2 \left(\frac{(\Delta x)_I}{(\Delta x)_{DF}} \right) a \frac{d^2}{dt^2} \widetilde{T}_o + \frac{2}{3} a \frac{d}{dt} \widetilde{T}_o + \frac{4}{3} a \widetilde{T}_o = 0$$

describing a damped oscillation $\widetilde{T}_o(t) \sim e^{\gamma t + i\omega t}$ with

$$\gamma = -\frac{(\Delta x)_I \cdot (\Delta x)_{DF}}{2\chi(\Delta t)^2}$$

and a frequency given – in the most relevant case of $\Delta t \gg \frac{\sqrt{(\Delta x)_I (\Delta x)_{DF}}}{2\sqrt{2}\chi}$ – by

$$\omega = \frac{\sqrt{2(\Delta x)_I \cdot (\Delta x)_{DF}}}{a(\Delta t)}.$$

The above procedure – using the approximate spatial form of the numerically found dominating perturbation as a trial function to construct a Galerkin procedure – can be applied also to other perturbations, excited, e.g. by a bad initialisation of the DF points. The resulting expressions for damping rates and frequencies take the general form

$$\gamma = -c_1 \frac{(\Delta x)_I \cdot (\Delta x)_{DF}}{2\chi(\Delta t)^2},$$

$$\omega = c_2 \frac{\sqrt{2(\Delta x)_I \cdot (\Delta x)_{DF}}}{\ell(\Delta t)},$$

already described in the text, with ℓ the characteristic space scale of the perturbation. Common to all the perturbations is their nearly polygonal form, with straight sections connecting the DF points.

References

[1] S. Günter et al., J. Comp. Phys. 209 (2005) 354.
[2] S. Günter, Ch. Tichmann, K. Lackner, J. Comp. Phys. 226 (2007) 2306.
[3] M. Hölzl, S. Günter, K. Lackner, Phys. Plasmas 14 (2007) 052501.
[4] Q. Yu et al., Nucl. Fusion 48 (2008) 024007.
[5] M. Hölzl et al., Phys. Plasmas 15 (2008) 072514.
[6] G. Yuan, F. Zuo, Int. J. Comput. Math. 80 (2003) 993–997.
[7] K. Black, J. Sci. Comput. 7 (1992) 313–338.
[8] Yu. I. Shokin, The Method of Differential Approximation, Springer-Verlag, New York, 1983.